Available online at www.sciencedirect.com
SCIENCE DIRECT
Journal of Computational Physics 216 (2006) 195–215
JOURNAL OF COMPUTATIONAL PHYSICS
www.elsevier.com/locate/jcp

A semi-Lagrangian discontinuous Galerkin method for scalar advection by incompressible flows

M. Restelli [a,*], L. Bonaventura [a], R. Sacco [b]

[a] *MOX – Modellistica e Calcolo Scientifico, Dipartimento di Matematica "F. Brioschi", Politecnico di Milano, via Bonardi 9 20133 Milano, Italy*
[b] *Dipartimento di Matematica "F. Brioschi", Politecnico di Milano, via Bonardi 9 20133 Milano, Italy*

Received 8 June 2005; received in revised form 25 November 2005; accepted 28 November 2005
Available online 18 January 2006

Abstract

A new, conservative semi-Lagrangian formulation is proposed for the discretization of the scalar advection equation in flux form. The approach combines the accuracy and conservation properties of the Discontinuous Galerkin (DG) method with the computational efficiency and robustness of Semi-Lagrangian (SL) techniques. Unconditional stability in the von Neumann sense is proved for the proposed discretization in the one-dimensional case. A monotonization technique is then introduced, based on the Flux Corrected Transport approach. This yields a multi-dimensional monotonic scheme for the piecewise constant component of the computed solution that is characterized by a smaller amount of numerical diffusion than standard DG methods. The accuracy and stability of the method are further demonstrated by two-dimensional tracer advection tests in the case of incompressible flows. The comparison with results obtained by standard SL and DG methods highlights several advantages of the new technique.

Keywords: Advection equation; Conservative tracer transport; Flux form semi-Lagrangian techniques; Discontinuous Galerkin finite element method

1. Introduction

The development of accurate and conservative numerical methods to solve efficiently the linear advection equation

$$\frac{\partial c}{\partial t} + \operatorname{div}(\mathbf{u}c) = 0 \tag{1}$$

has always been a main goal of the research on advection dominated flows. In this context, the semi-Lagrangian (SL) method is widely acknowledged as an accurate and efficient option [13,35,45]. In SL methods, Eq. (1) is reformulated in Lagrangian form

* Corresponding author. Fax: +39 02 23994606.
E-mail addresses: marco.restelli@mate.polimi.it (M. Restelli), luca.bonaventura@polimi.it (L. Bonaventura), riccardo.sacco@mate.polimi.it (R. Sacco).

0021-9991/$ - see front matter © 2005 Elsevier Inc. All rights reserved.
doi:10.1016/j.jcp.2005.11.030

$$\frac{\mathrm{d}c}{\mathrm{d}t} = \frac{\partial c}{\partial t} + \mathbf{u} \cdot \nabla c = -c \operatorname{div} \mathbf{u}, \tag{2}$$

and time discretization exploits the fact that the solution values are available along the characteristic lines, which are approximated numerically [44]. The original formulation of SL methods, however, is inherently nonconservative, so that, in order to achieve local mass conservation, two main approaches are typically pursued.

In the first strategy, based on conservative remapping [24], Eq. (2) is formally integrated over a control volume that is *moving with the flow*, and then discretized by approximate reconstruction of the upstream control volume (see [26,32,33,38,50] for examples of mass conserving variants of the SL method based on remapping). In the second strategy, more similar in spirit to Eulerian finite volume methods, Eq. (1) is first integrated in space over a *fixed mesh control volume*. It is then integrated in time over a time step Δt, and finally it is discretized by approximate reconstruction of the flux through the control volume boundary over Δt. The resulting methods can be referred to as flux form SL schemes (see e.g. [12,15–19,28,30,31]; see also [35], for a description and stability analysis of these approaches as generalized Godunov methods). Flux form SL schemes can also be interpreted as a natural generalization of wave propagation methods, see, e.g., [29].

The purpose of the present work is to introduce a flux form SL discretization for (1) that employs a Discontinuous Galerkin (DG) formulation [8,10] to reconstruct the numerical solution within each control volume. Throughout the paper, the novel technique is referred to as semi-Lagrangian Discontinuous Galerkin (SLDG) approach. The properties of the proposed method are analyzed here assuming the advective flow $\mathbf{u}$ in (1) to be incompressible. One possible approach to include diffusive terms in the mathematical model is also discussed in the present work, although a full understanding of the optimal way to treat diffusion in conjunction with SLDG requires further study. Another issue that is currently being investigated concerns the coupling of the SLDG formulation with other discretizations of compressible fluid flow equations.

The SLDG method aims at combining the accuracy and conservation property of the DG method with the computational efficiency and robustness of SL techniques. On one hand, the use of SL backward trajectories allows to achieve unconditional stability, irrespective of the value of the Courant number, thus overcoming the severe stability restrictions enforced by the DG formulation. On the other hand, the potential loss of accuracy of standard SL methods at low Courant numbers pointed out in [14] does not affect the SLDG scheme, as demonstrated by a number of numerical experiments. Furthermore, in the case of large systems of advection–diffusion–reaction equations, as typical of environmental modelling applications [25,48], the extra effort needed to compute the trajectories is required only once for the whole system, so that the potential overhead associated with this effort becomes negligible, as demonstrated in [31]. Finally, the proposed method is characterized by a computational stencil that is similar to those of standard Eulerian DG formulation. This means that high order approximations can be constructed locally, without involving a large number of neighbouring elements, thus making domain decomposition-based parallelization approaches more straightforward. As it will be clear from the description of the numerical method, the use of an elementwise variable-degree formulation is also possible, leaving unaltered the global and local mass conservation properties of the scheme. This feature of the formulation will be exploited in a future improved implementation of the scheme to reduce computational costs.

A brief outline of the article is as follows. The SLDG method is described in Section 2. A von Neumann stability analysis for the constant coefficient, one-dimensional case is then carried out in Section 3, showing that the method is stable for arbitrary values of the Courant number. Since the SLDG is not inherently monotonic in its higher order version, a monotonization approach based on the Flux Corrected Transport (FCT) technique is introduced and discussed in Section 4, while in Section 5 the interesting properties of the new method are demonstrated by a number of numerical tests relevant in advection dominated flows. Future developments and possible applications are finally discussed in Section 6.

2. The semi-Lagrangian discontinuous Galerkin method

In this section we describe in detail the Semi-Lagrangian Discontinuous Galerkin (SLDG) method. In doing this, we combine the unified framework for generalized Godunov methods proposed in [35] with the

Discontinuous Galerkin finite element formulation introduced and analyzed in [8,10] in the case of nonlinear hyperbolic problems.

2.1. Preliminaries

Let Ω be an open bounded domain of $\mathbb{R}^2$, with boundary $\partial\Omega \equiv \Gamma$ and outward unit normal vector $\mathbf{n}_\Gamma$, where a solution of (1) is to be approximated, and let $\mathscr{T}_h$ denote a partition of Ω into N_{el} triangular elements K. This latter choice allows an easy generation of approximation basis functions of arbitrary polynomial order and provides a great flexibility to the geometrical discretization of the computational domain. The application of the scheme to include quadrilateral elements and to treat three-dimensional problems can be carried out along the same lines as in [21,22].

The area of an element K is denoted by $|K|$, while its boundary and outward unit normal vector are ∂K and $\mathbf{n}_{\partial K}$, respectively. The diameter of K is h_K and $h = \max_{K\in\mathscr{T}_h} h_K$. The set of all the edges of K is $\mathscr{E}_K$, while $\mathscr{E}_h$ is the set of the N_{edges} edges of the triangulation, $|e|$ denoting the length of a generic edge $e \in \mathscr{E}_h$. For each internal edge $e \in \mathscr{E}_h$, a normal unit vector $\mathbf{n}_e$ is arbitrarily fixed, and K_e^1, K_e^2 denote the two elements of $\mathscr{T}_h$ sharing the edge e and such that $\mathbf{n}_e$ is directed from K_e^1 to K_e^2. If $e \in \Gamma$, then $\mathbf{n}_e \equiv \mathbf{n}_\Gamma$ and K_e^1 is the element of $\mathscr{T}_h$ having e as a boundary edge. Consistently, let $\sigma_{K_e^1,e} = 1$ and $\sigma_{K_e^2,e} = -1$, in such a way that $\sigma_{K_e^i,e}\mathbf{n}_e$ is the outer normal unit vector associated with edge e of element K_e^i for $i = 1, 2$.

Let k be a nonnegative integer. Then $V_h(K) = \mathbb{P}_k(K)$ denotes the space of polynomials of degree at most k on element K, with $N_k \equiv \dim(V_h(K)) = \frac{1}{2}(k+1)(k+2)$. The space of elements of $L^\infty(\Omega)$ whose restriction to $K \in \mathscr{T}_h$ belongs to $V_h(K)$ is denoted by V_h. Notice that functions in V_h are in general discontinuous across each edge $e \in \mathscr{E}_h$.

Eq. (1) is to be approximated in Ω supplied with inflow boundary conditions and under the assumption that the given velocity vector field $\mathbf{u}$ is solenoidal, i.e., $\mathrm{div}\,\mathbf{u} = 0$ in (2). In view of the numerical approximation of Eq. (1), we need to introduce the *projection* of $\mathbf{u}$ over the finite element space of Raviart–Thomas of lowest degree [40]. With a slight abuse of notation, we indicate throughout the article this projection by the symbol $\mathbf{u}$. The numerical importance of using this projected field relies on the fact that (i) it allows an *automatic* flux conservation across interelement boundaries and (ii) it is easy to check that $\mathbf{u}$ is *piecewise constant* on each $K \in \mathscr{T}_h$. The construction of $\mathbf{u}$ only requires for each edge $e \in \mathscr{E}_h$ the constant quantity u_e, that is the normal velocity component in the direction of $\mathbf{n}_e$. Then, for each time interval $[t^n, t^{n+1}]$, with $\Delta t = t_{n+1} - t_n$, the normal components of the velocity field to the edges of $\mathscr{T}_h$ are assumed to be given at the intermediate time level $t^{n+\frac{1}{2}}$ and are denoted by $u_e^{n+\frac{1}{2}}$, $e = 1, \ldots, N_{\mathrm{edges}}$, so that the (discrete) divergence free constraint amounts to requiring that

$$\sum_{e\in\mathscr{E}_K} \sigma_{K,e} u_e^{n+\frac{1}{2}} |e| = 0 \quad \forall K \in \mathscr{T}_h. \tag{3}$$

The time dependence of $\mathbf{u}$ and u_e will often be omitted in the following for the sake of simplicity. We notice that assuming that $\mathbf{u}$ can be completely determined by its normal fluxes eases the future coupling of the proposed scheme to mass conservative methods for environmental flows, such as those proposed in [4–6,34]. Moreover, assuming a velocity field piecewise constant in time, although limiting a priori the formal accuracy of the method, corresponds to what is actually computationally feasible when coupling tracer advection to most semi-Lagrangian models for fluid flow.

2.2. Spatial discretization

The spatial discretization of (1) is carried out initially along the usual lines of Discontinuous Galerkin (DG) methods (see e.g. [8]). An approximation $c_h = c_h(x, t)$ to the solution $c(x, t)$ of (1) is sought, such that $c_h \in V_h$ at each time level. Multiplying Eq. (1) by a function $v_h \in V_h$, integrating over $K \in \mathscr{T}_h$ and replacing the exact solution c by its approximation c_h, we get

$$\frac{\mathrm{d}}{\mathrm{d}t}\int_K c_h(x,t)v_h(x)\,\mathrm{d}x = -\int_K \mathrm{div}(\mathbf{u}(x,t)c_h(x,t))v_h(x)\,\mathrm{d}x \quad \forall v_h \in V_h.$$

Then, formally integrating by parts, we obtain

$$\frac{\mathrm{d}}{\mathrm{d}t}\int_K c_h(x,t)v_h(x)\,\mathrm{d}x = \int_K c_h(x,t)\mathbf{u}(x,t)\cdot\nabla v_h(x)\,\mathrm{d}x - \int_{\partial K} c_h(\xi,t)\mathbf{u}(\xi,t)\cdot\mathbf{n}_{\partial K}v_h(\xi)\,\mathrm{d}\xi \quad \forall v_h \in V_h. \tag{4}$$

Notice that the advective boundary term $c_h(\xi, t)\mathbf{u}\cdot\mathbf{n}_{\partial K}$ in (4) does not yet have a precise meaning, because c_h is a discontinuous function across interelement boundaries. Eq. (4) is the starting point for time discretization with Runge–Kutta schemes in standard DG formulations [8,10]. In our approach, we depart from this latter procedure and follow the path of generalized Godunov methods as presented and analyzed in [35]. With this aim, we integrate (4) in time between t^n and t^{n+1}, to obtain the following weak form of the linear advection equation:

$$\begin{aligned}\int_K c_h(x,t^{n+1})v_h(x)\,\mathrm{d}x = &\int_K c_h(x,t^n)v_h(x)\,\mathrm{d}x + \int_{t^n}^{t^{n+1}}\mathrm{d}\tau\int_K c_h(x,\tau)\mathbf{u}(x,\tau)\cdot\nabla v_h(x)\,\mathrm{d}x\\ &- \int_{t^n}^{t^{n+1}}\mathrm{d}\tau\int_{\partial K} c_h(\xi,\tau)\mathbf{u}(\xi,\tau)\cdot\mathbf{n}_{\partial K}v_h(\xi)\,\mathrm{d}\xi \quad \forall v_h \in V_h.\end{aligned} \tag{5}$$

For each element $K \in \mathscr{T}_h$, the discrete degrees of freedom associated with the numerical solution at a given time level t^n are denoted by $\{c^n_{j,K}\}_{j\in\mathscr{J}_k}$, with $\mathscr{J}_k = \{0,\ldots,N_k-1\}$, so that an approximate numerical solution can be reconstructed locally for all $K \in \mathscr{T}_h$ as

$$c_h(x,t^n)|_K = \sum_{j\in\mathscr{J}_k} c^n_{j,K}\phi_{j,K}(x). \tag{6}$$

In the following, the functions $\phi_{j,K}(x)$ are taken to be an orthogonal basis for $\mathbb{P}_k(K)$ such that $\int_K\phi_{i,K}(x)\phi_{j,K}(x)\mathrm{d}x = |K|\delta_{ij}$ (and, in particular, $\phi_{0,K}(x) = \mathbb{1}_K(x)$, $\mathbb{1}_K$ being the characteristic function associated with element K, and $\int_K\phi_{j,K}(x)\mathrm{d}x = 0$ for $j > 0$). For brevity, we set henceforth $c^n_h(x) = c_h(x,t^n)$.

2.3. Time discretization

The next step is to derive from (5) a full space–time discretization. In order to describe the time evolution of $c_h(x, t)$, we define, as in [35], the exact evolution operator

$$E(t,s) : c(x,t) \to [E(t,s)c(\cdot,t)](x) = c(x,t+s). \tag{7}$$

$E(t, s)$ can be interpreted as a representation of the solution of the linear advection equation in *nonconservative* form (2). More precisely, under mild regularity assumptions on the velocity field (see [39]), it can be proven that streamline or characteristic line functions exist, which are defined as the solutions of the ordinary differential equations

$$\frac{\mathrm{d}}{\mathrm{d}s}X(x,t;t+s) = \mathbf{u}(X(x,t;t+s),t+s) \tag{8}$$

with initial datum at time t given by $X(x, t\,; t) = x$. For smooth and solenoidal given velocity $\mathbf{u}$, by the chain rule it is then possible to prove that for any t and s the following relation holds:

$$c(x,t+s) = [E(t,s)c(\cdot,t)](x) = c(X(x,t+s;t),t). \tag{9}$$

A discrete approximation of this evolution operator representing the time evolution from a time level t^n to $t^n + s$ is denoted by E^n_s. Providing a discrete approximation $\widehat{X}(x,t;t+s)$ for the solution of (8), with $s \in [0, \Delta t]$, completely determines the operator E^n_s as

$$\left[E^n_s c^n_h\right](x) = c^n_h(\widehat{X}(x,t^n+s;t^n)). \tag{10}$$

Function $\widehat{X}$ can be interpreted as the numerical approximation of the streamlines usually performed in semi-Lagrangian methods. Following the ideas proposed in [28,30], we can now use (9) and (10) to evaluate the right hand side of (5), so that the SLDG method can be defined for each element $K \in \mathscr{T}_h$ by

$$|K|c_{j,K}^{n+1} = |K|c_{j,K}^{n} + \int_0^{\Delta t} \mathrm{d}s \int_K \left[E_s^n c_h^n\right](x)\mathbf{u}\left(x, t^{n+\frac{1}{2}}\right)\cdot\nabla\phi_{j,K}(x)\,\mathrm{d}x - \int_0^{\Delta t}\mathrm{d}s \sum_{e\in\mathscr{E}_K}\int_e \left[E_s^n c_h^n\right](\xi)u_e^{n+\frac{1}{2}}\phi_{j,K}(\xi)\,\mathrm{d}\xi \quad \forall j\in\mathscr{J}_k. \tag{11}$$

For ease of notation, the time dependency of the velocity field will be omitted in the remainder of the article.

2.4. The fully discrete SLDG approximation

In order to obtain a fully discrete method, the integrals in space and time in (11) must be replaced by appropriate quadrature rules. In the present implementation of the proposed method, Gaussian quadrature rules are used for the integration in space. Gaussian points $\{x_v\}_{v=1}^{L_e}$, $\{y_v\}_{v=1}^{L_f}$, are introduced on the edges and the elements, respectively. The corresponding Gaussian weights are denoted by $\{\tilde{\omega}_v\}_{v=1}^{L_e}$, $\{\tilde{\tilde{\omega}}_v\}_{v=1}^{L_f}$. For the integration in time, a simple composite rule is applied in the present implementation. For each element K and for each edge e, we define intermediate time levels $\{s_m^K\}_{m=0}^{M(K)}$, $\{s_m^e\}_{m=0}^{M(e)}$. For convenience, the dependency on the edge and element is often dropped and should be recovered from the context. The intermediate time levels are such that $s_0 = 0$, $s_M = \Delta t$ and $\Delta s_m = s_m - s_{m-1}$. Formally, we make the approximation

$$\int_0^{\Delta t} E_s^n\,\mathrm{d}s \approx \sum_{m=0}^{M-1} E^n_{s_{m+\frac{1}{2}}}\Delta s_m, \tag{12}$$

where now $s_{m+\frac{1}{2}} = s_m + \frac{\Delta s_m}{2}$. More accurate composite integration rules can of course be used along the same lines. The numerical trajectories $\widehat{X}(x, t^n + s; t^n)$ necessary for the complete definition of E_s^n are computed by a simple backward Euler method with time substeps given by the quantities Δs_m. Given these definitions, the fully discrete SLDG approximation of Eq. (1) can then be defined for each $K\in\mathscr{T}_h$ as

$$|K|c_{j,K}^{n+1} = |K|c_{j,K}^{n} + \sum_{m=0}^{M-1}\sum_{v=1}^{L_f}\left[E^n_{s_{m+\frac{1}{2}}}c_h^n\right](y_v)\mathbf{u}(y_v)\cdot\nabla\phi_{j,K}(y_v)\Delta s_m\tilde{\tilde{\omega}}_v - \sum_{e\in\mathscr{E}_K}\sigma_{K,e}u_e|e|\sum_{m=0}^{M-1}\sum_{v=1}^{L_e}\left[E^n_{s_{m+\frac{1}{2}}}c_h^n\right](x_v)\phi_{j,K}(x_v)\Delta s_m\tilde{\omega}_v \quad \forall j\in\mathscr{J}_k. \tag{13}$$

It must be remarked that the approximation (12) of the evolution operator eliminates the ambiguity in the definition of the numerical fluxes along interelement boundaries, since in all cases with nonzero advecting velocity the quantity $[E^n_{s_{m+\frac{1}{2}}}c_h^n](x_v)$ is uniquely defined for $m = 0, \ldots, M-1$. In the special case where piecewise constant finite elements are considered, the following finite volume method is recovered from (13):

$$|K|c_{0,K}^{n+1} = |K|c_{0,K}^{n} - \sum_{e\in\mathscr{E}_K}\sigma_{K,e}u_e|e|\sum_{m=0}^{M-1}\sum_{v=1}^{L_e}\left[E^n_{s_{m+\frac{1}{2}}}c_h^n\right](x_v)\Delta s_m\tilde{\omega}_v, \tag{14}$$

where the quantity $c_{0,K}^n$ is the discrete degree of freedom representing the average of the concentration over element $K\in\mathscr{T}_h$ and c_h^n is a piecewise constant function over $\mathscr{T}_h$.

3. Linear stability analysis in the one-dimensional case

In this section, we carry out along the lines of [7] the stability analysis of the SLDG scheme in the von Neumann sense. The proof will be given only for the case of linear polynomial approximations $\mathbb{P}_1$. With this aim, let us consider Eq. (1) in the one-dimensional case with constant advection velocity

$$\begin{cases} c_t + uc_x = 0 & \text{in } [0,L]\times[0,T], \\ c(x,0) = c_0(x) & x\in[0,L], \end{cases} \tag{15}$$

and supplied with periodic initial and boundary conditions. Let $\mathscr{T}_h$ be a uniform partition of $[0, L]$ into elements $K_j = (x_{j-1/2}, x_{j+1/2})$ of size h, and Δt denote the time step. Moreover, for each $K_j\in\mathscr{T}_h$, let x_j be

the midpoint of K_j. The key stability parameter is the Courant number $C = \frac{u\Delta t}{h}$, which can be split into its integer and fractional part as $C = m + \gamma$, with $m \in \mathbb{N}$ and $\gamma \in [0, 1)$, as customary in the analysis of semi-Lagrangian schemes (see e.g. [2]). Introducing the cell characteristic time $\tau = \frac{h}{u}$ we have also $\Delta t = (m + \gamma)\tau$. Denoting now by a_j and b_j the degrees of freedom of c_h with respect to the $\mathbb{P}_1$ hierarchical basis, we have

$$c_h^n(x)\big|_{K_j} = a_j^n + 6b_j^n(x - x_j)/(\sqrt{3}h) \quad \forall K_j \in \mathscr{T}_h.$$

The SLDG formulation (13) for the evolution of c_h from time level t^n to t^{n+1} can then be expressed as a function of a_j and b_j as

$$\begin{aligned} a_j^{n+1} &= a_{j-m}^n - \gamma\left(a_{j-m}^n - a_{j-m-1}^n\right) - \sqrt{3}\gamma(1-\gamma)\left(b_{j-m}^n - b_{j-m-1}^n\right), \\ b_j^{n+1} &= b_{j-m}^n + \sqrt{3}\gamma(1-\gamma)\left(a_{j-m}^n - a_{j-m-1}^n\right) - 3\gamma(1-\gamma)\left(b_{j-m}^n + b_{j-m-1}^n\right) - 2\gamma^2\left(\frac{3}{2} - \gamma\right)\left(b_{j-m}^n - b_{j-m-1}^n\right). \end{aligned} \tag{16}$$

Proposition 3.1. *The SLDG method (16) is unconditionally L^2-stable.*

Proof. We have

$$\left\|c_h^n\right\|_{L^2(0,L)}^2 = h\sum_j \left\{\left(a_j^n\right)^2 + \left(b_j^n\right)^2\right\}. \tag{17}$$

We can associate with c_n^h the piecewise constant vector function $[a_h^n(x), b_h^n(x)]^{\mathrm{T}}$ with $a_h^n(x) = \sum_j a_j^n \mathbb{1}_{K_j}(x)$ and $b_h^n(x) = \sum_j b_j^n \mathbb{1}_{K_j}(x)$, so that (17) can be rewritten as

$$\left\|c_h^n\right\|_{L^2(0,L)}^2 = \left\|a_h^n\right\|_{L^2(0,L)}^2 + \left\|b_h^n\right\|_{L^2(0,L)}^2. \tag{18}$$

Let us consider the Fourier series $a_h^n(x) = \sum_{k\in\mathbb{Z}} A_k^n \mathrm{e}^{\mathrm{I}\frac{2k\pi}{L}x}$ and $b_h^n(x) = \sum_{k\in\mathbb{Z}} B_k^n \mathrm{e}^{\mathrm{I}\frac{2k\pi}{L}x}$ associated with a_h^n and b_h^n, where $\mathrm{I} = \sqrt{-1}$. Applying the Bessel–Parseval equality to (18) yields

$$\left\|c_h^n\right\|_{L^2(0,L)}^2 = L\sum_{k\in\mathbb{Z}}\left(\left|A_k^n\right|^2 + \left|B_k^n\right|^2\right). \tag{19}$$

The coefficients A_k^{n+1}, B_k^{n+1} of the SLDG method can be expressed as linear combinations of A_k^n, B_k^n as follows:

$$\left[A_k^{n+1}, B_k^{n+1}\right]^{\mathrm{T}} = \mathrm{e}^{-\mathrm{I}\theta m}\mathbf{G}(\theta,\gamma)\left[A_k^n, B_k^n\right]^{\mathrm{T}}, \tag{20}$$

where $\theta = \frac{2k\pi h}{L}$ and $\mathbf{G}$ is the skew-symmetric amplification matrix with entries

$$\begin{aligned} G_{11}(\theta,\gamma) &= 1 - \gamma(1 - \mathrm{e}^{-\mathrm{I}\theta}), \quad G_{12}(\theta,\gamma) = -\sqrt{3}\gamma(1-\gamma)(1 - \mathrm{e}^{-\mathrm{I}\theta}), \\ G_{22}(\theta,\gamma) &= 1 - 3\gamma(1-\gamma)(1 + \mathrm{e}^{-\mathrm{I}\theta}) - \gamma^2(3 - 2\gamma)(1 - \mathrm{e}^{-\mathrm{I}\theta}). \end{aligned}$$

Let $\lambda_{1,2}$ denote the eigenvalues of $\mathbf{G}$, with $|\lambda_2| \leqslant |\lambda_1|$. It can be checked that $\lambda_1 \neq \lambda_2$ for all $\theta \in [-\pi, \pi]$, and that for $\theta \to 0$,

$$|\lambda_1| = 1 - \frac{1}{72}\gamma(1-\gamma)(1 - \gamma + \gamma^2)\theta^4 + \mathscr{O}(\theta^6),$$

so that, $\forall\theta \in [-\pi, \pi]$ we have $|\lambda_1| < 1$ for $|\gamma| \leqslant 1$, as can be seen from the plots of λ_1, λ_2 in Fig. 1. As a consequence, the following inequality holds:

$$\left\|c_h^{n+1}\right\|_{L^2(0,L)}^2 < \left\|c_h^n\right\|_{L^2(0,L)}^2$$

which proves the unconditional stability of the SLDG method in the von Neumann sense. □

We notice that the stability result proved in this section is analogous to what is usually obtained for standard SL methods (see e.g. [2,14]), and it provides an improvement of the stability analysis carried out in [9], which yields the stability constraint $\gamma < \frac{1}{3}$ for the DG method using linear finite elements.

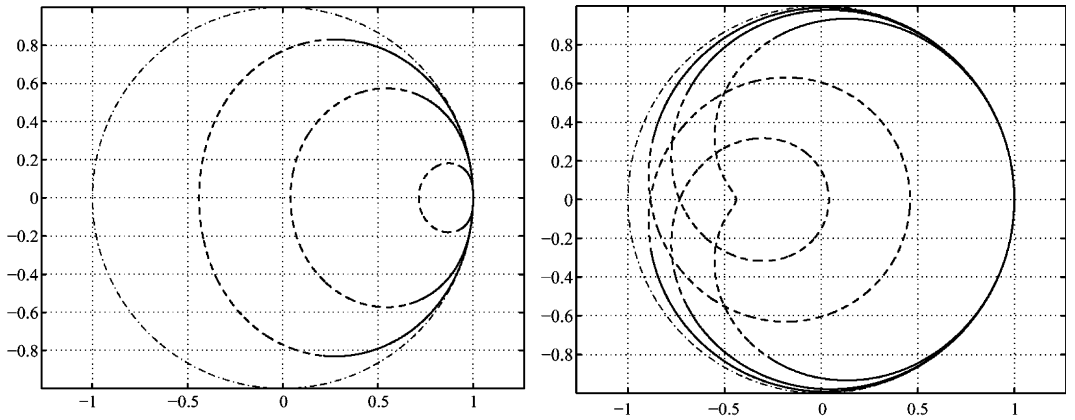

Fig. 1. Plot of λ_1 (solid line) and λ_2 (dashed line) for $\gamma = 0.05, 0.2, 0.4$ (left) and $\gamma = 0.6, 0.8, 0.9$ (right). Dash–dot line: unit circle.

4. Monotonicity

In this section, we provide a technique to make the SLDG discretization (13) a monotonic method. In order to achieve this important property, we first show in Section 4.2 that the piecewise constant part of the approximate solution satisfies a discrete maximum principle, that is

$$\min_{K\in\mathscr{T}_h} c^n_{0,K} \leqslant c^{n+1}_{0,K} \leqslant \max_{K\in\mathscr{T}_h} c^n_{0,K} \quad \forall K \in \mathscr{T}_h. \tag{21}$$

Then, we apply to the SLDG formulation the well known Flux Corrected Transport (FCT) technique [49] to enforce monotonicity of the higher order approximate solution. It is important to notice that, as in the context of DG methods for scalar conservation laws, the proof of a discrete maximum principle is divided into two steps [8]. In the first step, a discrete maximum principle is proved for the degrees of freedom representing the average of the solution over each element K (i.e., in our case, the values $c^{n+1}_{0,K}$). Then, a discrete maximum principle is established for the DG method using higher order elements by limiting the slopes of the numerical solution, represented by the degrees of freedom $c^n_{j,K}$, with $j = 1, \ldots, N_k - 1$, in (6). In the present approach, instead, we enforce monotonicity by a suitable correction of the edge flux contributions in (11) using the FCT approach, as explained in Section 4.3.

4.1. Definition of edge fluxes

In this preliminary section, we introduce edge fluxes into the SLDG formulation (13). For each edge $e \in \partial K$, we define the approximate flux associated with the jth degree of freedom as

$$F^j_e = u_e|e| \sum_{m=0}^{M-1} \sum_{v=1}^{L_e} \left[E^n_{s_{m+\frac{1}{2}}} c^n_{h,j} \right](x_v) \Delta s_m \tilde{\omega}_v \quad \forall j \in \mathscr{J}_k,$$

where $c^n_{h,j}(x) = \sum_{K\in\mathscr{T}_h} c^n_{j,K} \phi_{j,K}(x)$ represents the jth component of $c^n_h(x)$. Using the above definition, the update (14) for the mean value of c_h can be written in the following equivalent form:

$$c^{n+1}_{0,K} = c^n_{0,K} - \sum_{e\in\mathscr{E}_K} \frac{\sigma_{K,e} u_e |e|}{|K|} \sum_{m=0}^{M-1} \sum_{v=1}^{L_e} \left[E^n_{s_{m+\frac{1}{2}}} c^n_h \right](x_v) \Delta s_m \tilde{\omega}_v = c^n_{0,K} - \sum_{e\in\mathscr{E}_K} \frac{\sigma_{K,e}}{|K|} F^0_e - \sum_{j=1}^{N_k-1} \sum_{e\in\mathscr{E}_K} \frac{\sigma_{K,e}}{|K|} F^j_e. \tag{22}$$

It is now convenient to redefine F^0_e as

$$F^0_e = \int_0^{\Delta t} \mathrm{d}s \int_e \left[E^n_s c^n_{h,0} \right](\xi)\, \mathrm{d}\xi = \int_e \mathrm{d}\xi \int_0^{\Delta t} \left[E^n_s c^n_{h,0} \right](\xi)\, \mathrm{d}s. \tag{23}$$

Due to (10), one has

$$\int_0^{\Delta t} \left[E_s^n c_{h,0}^n\right](\xi)\,\mathrm{d}s = \int_0^{\Delta t} c_{h,0}^n(\widehat{X}(\xi, t^n + s; t^n))\,\mathrm{d}s.$$

It must be remarked that, since the time dependency of the velocity field is assumed to be frozen during each time step, the set of points $\widehat{X}(\xi, t^n + s; t^n)$, $s \in [0, \Delta t]$, coincides with those spanned by the backward trajectory $\widehat{X}(\xi, t^{n+1}; t^{n+1} - s)$, $s \in [0, \Delta t]$. Noting that $c_{h,0}^n$ is piecewise constant over $\mathscr{T}_h$, the previous relation can be written as

$$\int_0^{\Delta t} c_{h,0}^n(\widehat{X}(\xi, t^n + s; t^n))\,\mathrm{d}s = \sum_{K'} c_{0,K'}^n \Delta s_{K'}^{\xi},$$

where $\Delta s_{K'}^{\xi}$ denotes the amount of time during which $\widehat{X}(\xi, t^{n+1}; t^{n+1} - s) \in K'$ and the sum is extended over all elements crossed by $\widehat{X}(\xi, t^{n+1}; t^{n+1} - s)$. As a result, $\sum_{K'} \Delta s_{K'}^{\xi} = \Delta t$ independently of ξ and

$$F_e^0 = u_e |e| \Delta t \sum_{K' \in \mathscr{T}_e} \alpha_{K',e} c_{0,K'}^n, \tag{24}$$

where we set

$$\alpha_{K',e} = \frac{1}{|e|\Delta t} \int_e \Delta s_{K'}^{\xi}\,\mathrm{d}\xi \tag{25}$$

and where $\mathscr{T}_e$ is the set of all elements crossed by $\widehat{X}(\xi, t^{n+1}; t^{n+1} - s)$ for any $\xi \in e$. Noting that for each edge $e \in \mathscr{E}_K$ we have

$$\sum_{K'} \int_e \Delta s_{K'}^{\xi}\,\mathrm{d}\xi = |e|\Delta t,$$

from definition (25) it turns out that $\alpha_{K',e} \geqslant 0$ and

$$\sum_{K' \in \mathscr{T}_e} \alpha_{K',e} = 1. \tag{26}$$

Furthermore, in the case of a velocity field defined as in Section 2.1 and satisfying exactly the discrete divergence free constraint (3), the quantities $\Delta s_{K'}^{\xi}$ and $\alpha_{K',e}$ can be computed exactly.

4.2. Monotonicity of $c_{h,0}$

In this section, we carry out the first step of the monotonicity proof by showing that the mean value of c_h, defined as

$$c_{0,K}^{n+1} = c_{0,K}^n - \sum_{e \in \mathscr{E}_K} \frac{\sigma_{K,e}}{|K|} F_e^0, \tag{27}$$

satisfies the discrete maximum principle.

Proposition 4.1. *The quantity $c_{0,K}^{n+1}$ satisfies the discrete maximum principle (21).*

Proof. Let us show that the update $c_{0,K}^{n+1}$ can be expressed as a linear combination of $c_{0,K'}^n$ with nonnegative coefficients. With this aim, we introduce the following sets:

$$\mathscr{E}_K^+ = \{e \in \mathscr{E}_K : \sigma_{K,e} u_e \geqslant 0\}, \quad \mathscr{E}_K^- = \{e \in \mathscr{E}_K : \sigma_{K,e} u_e < 0\},$$

which represent the outflow and inflow boundaries of K, respectively. We also introduce the two following subsets of $\mathscr{T}_e$

$$\mathscr{T}_K^+ = \bigcup_{e \in \mathscr{E}_K^+} \mathscr{T}_e, \quad \mathscr{T}_K^- = \bigcup_{e \in \mathscr{E}_K^-} \mathscr{T}_e.$$

Clearly, $\mathscr{E}_K = \mathscr{E}_K^+ \cup \mathscr{E}_K^-$, which can be used to reformulate (27) as

$$c_{0,K}^{n+1} = c_{0,K}^n - \sum_{K' \in \mathscr{T}_K^+} \sum_{e \in \mathscr{E}_K^+} \frac{|u_e||e|\Delta t}{|K|} \alpha_{K',e} c_{0,K'}^n + \sum_{K' \in \mathscr{T}_K^-} \sum_{e \in \mathscr{E}_K^-} \frac{|u_e||e|\Delta t}{|K|} \alpha_{K',e} c_{0,K'}^n. \tag{28}$$

For simplicity, we make now the assumption that $K \notin \mathscr{T}_K^-$, which excludes the case of very high Courant numbers or flows with very strong deformation (i.e., high Lipschitz numbers according to the definition in [44]). The proof can be extended to cover also these cases, but it is far simpler under the above assumption. In any case, irrespective of this restriction, one has $\mathscr{T}_K^+ = \{K\} \cup (\mathscr{T}_K^+ \cap \mathscr{T}_K^-)$. Relation (28) can then be rewritten as

$$c_{0,K}^{n+1} = \alpha_K^n c_{0,K}^n + \sum_{K' \in (\mathscr{T}_K^- \cap \mathscr{T}_K^+)} \beta_{K'}^n c_{0,K'}^n + \sum_{K' \in (\mathscr{T}_K^- \setminus \mathscr{T}_K^+)} \gamma_{K'}^n c_{0,K'}^n \quad \forall K \in \mathscr{T}_h, \tag{29}$$

where

$$\alpha_K^n = \left(1 - \frac{\Delta t}{|K|} \sum_{e \in \mathscr{E}_K^+} |u_e||e|\alpha_{K,e}\right),$$

$$\beta_{K'}^n = \frac{\Delta t}{|K|} \left(\sum_{e \in \mathscr{E}_K^-} |u_e||e|\alpha_{K',e} - \sum_{e \in \mathscr{E}_K^+} |u_e||e|\alpha_{K',e}\right),$$

$$\gamma_{K'}^n = \frac{\Delta t}{|K|} \sum_{e \in \mathscr{E}_K^-} |u_e||e|\alpha_{K',e}.$$

Let us now show that α_K^n, $\beta_{K'}^n$ and $\gamma_{K'}^n$ are nonnegative and that

$$\alpha_K^n + \sum_{K' \in (\mathscr{T}_K^- \cap \mathscr{T}_K^+)} \beta_{K'}^n + \sum_{K' \in (\mathscr{T}_K^- \setminus \mathscr{T}_K^+)} \gamma_{K'}^n = 1. \tag{30}$$

To prove this latter property, let us first set $c_{0,J}^n = 1$ for all elements $J = K$, K' at the right hand side of (29). Then, (30) immediately follows using (26) and noting that

$$\frac{\Delta t}{|K|} \sum_{e \in \mathscr{E}_K} \sigma_{K,e}|u_e||e| = \frac{\Delta t}{|K|} \left[\sum_{e \in \mathscr{E}_K^-} |u_e||e| - \sum_{e \in \mathscr{E}_K^+} |u_e||e|\right] = 0.$$

Let us now check that the coefficients in (29) are nonnegative. This is immediate for $\gamma_{K'}^n$. For α_K^n, nonnegativity can be proved by using the definition of $s_{K'}^{\xi}$ and the properties of the Raviart–Thomas projection $\mathbf{u}$ discussed in Section 2.1. For $\beta_{K'}^n$, nonnegativity is ensured by the fact that, for an approximation of the characteristic lines based on the piecewise constant Raviart–Thomas projection $\mathbf{u}$, one has $\alpha_{K',e'} \geqslant \alpha_{K',e''}$ if $e' \in \mathscr{E}_K^-, e'' \in \mathscr{E}_K^+$. Then, for each $K' \in (\mathscr{T}_K^- \cap \mathscr{T}_K^+)$, we have

$$\sum_{e' \in \mathscr{E}_K^-} |u_{e'}||e'|\alpha_{K',e'} - \sum_{e'' \in \mathscr{E}_K^+} |u_e''||e''|\alpha_{K',e''} \geqslant \min_{e' \in \mathscr{E}_K^-} \alpha_{K',e'} \left[\sum_{e \in \mathscr{E}_K^-} |u_e||e| - \sum_{e \in \mathscr{E}_K^+} |u_e||e|\right].$$

Using again the fact that $\mathbf{u}$ satisfies (3), we immediately get that also $\beta_{K'}^n \geqslant 0$, which concludes the proof. □

4.3. Monotonicity of $c_{h,1}$ and $c_{h,2}$

In this section, we carry out the second step of the proof by deriving a monotonic higher order method through the use of the well known Flux Corrected Transport (FCT) technique (see [49]). In order to apply the FCT framework, we identify in (22) the quantities F_e^0 and $A_e = \sum_{j=1}^{N_k-1} F_e^j$ as low order diffusive flux and antidiffusive flux, respectively. Thus, appropriate limiting coefficients $C_e \in [0, 1]$ can be introduced for the antidiffusive fluxes in such a way to obtain the monotonized higher order scheme

$$c_{0,K}^{n+1} = c_{0,K}^n - \sum_{e \in \mathscr{E}_K} \frac{\sigma_{K,e}}{|K|} F_e^0 - \sum_{e \in \mathscr{E}_K} \frac{\sigma_{K,e}}{|K|} C_e A_e \quad \forall K \in \mathscr{T}_h. \tag{31}$$

The computation of the coefficients C_e is done along the same lines as in [49], and the algorithm is summarized here for sake of completeness.

For each $K \in \mathscr{T}_h$:

- compute the low order solution $\widetilde{c}_{0,K}^{n+1}$ using (31) with $A_e = 0$;
- compute the maximum and minimum allowable mean values $c_{0,K}^{\max}$ and $c_{0,K}^{\min}$ from the upstream neighboring elements;
- compute P_K^+ and P_K^- as the sum of all antidiffusive fluxes *into* and *away from* K, respectively;
- compute

$$Q_K^+ = \left(c_{0,K}^{\max} - \widetilde{c}_{0,K}^{n+1}\right)|K|, \quad Q_K^- = \left(\widetilde{c}_{0,K}^{n+1} - c_{0,K}^{\min}\right)|K|;$$

- set

$$R_K^+ = \begin{cases} \min\left(1, Q_K^+/P_K^+\right) & \text{if } P_K^+ > 0, \\ 0 & \text{if } P_K^+ = 0, \end{cases} \quad R_K^- = \begin{cases} \min\left(1, Q_K^-/P_K^-\right) & \text{if } P_K^- > 0, \\ 0 & \text{if } P_K^- = 0. \end{cases}$$

Finally, for each edge $e \in \mathscr{E}_h$, set

$$C_e = \begin{cases} \min\left(R_{K_e^2}^+, R_{K_e^1}^-\right) & \text{if } A_e \geqslant 0, \\ \min\left(R_{K_e^2}^-, R_{K_e^1}^+\right) & \text{if } A_e < 0. \end{cases}$$

5. Numerical results

In this section, we demonstrate the accuracy and stability of the SLDG method on one and two-dimensional benchmark test cases for passive tracer advection. Tests are performed for the plain, nonmonotonic (NM) and the FCT monotonized (M) versions of the SLDG method. A possible approach, based on a Discontinuous Galerkin formulation, is also proposed to include in SLDG the discretization of a diffusive term.

For the one-dimensional case, advection of both continuous and discontinuous profiles is considered. In order to compare the accuracy of the proposed SLDG scheme to that of well known reference schemes, the same test problems as in [23] are considered. Results indicate that the NM version of SLDG method is second and third order accurate when $\mathbb{P}_1$ and $\mathbb{P}_2$ elements are used, respectively. The M version of the scheme retains its accuracy away from local extrema (as usual for monotonic schemes); moreover, the absolute error values compare well with those reported in the reference.

For the two-dimensional case, we study solid body rotation and deformational flow tests for which analytic solutions are available. The results obtained using the SLDG method are then compared with those provided by its parent methods, e.g., the standard nonconservative semi-Lagrangian (SL) method and the Runge–Kutta Discontinuous Galerkin (RKDG) method. For the SL and SLDG runs the backward trajectories are approximated by using the backward Euler method with substepping (see e.g. [20,41]). These comparisons highlight several attractive properties of the SLDG formulation, which appears to merge effectively the SL and DG methods without any loss in accuracy. The FCT based monotonization approach described in Section 4 appears to be superior to the slope limiting approach proposed in [8] and does not exhibit the excessive sharpening of smooth profiles reported e.g. in [42] for more traditional applications of FCT. In particular, the idea of retaining higher order degrees of freedom in the computation of the monotonized flux for the piecewise constant component of c_h seems to be highly beneficial to the overall quality of the computed approximate solution, at least in the case of $\mathbb{P}_1$ elements.

In all the tests, the error norms $\|c - c_h\|_{L^2(\Omega)}/\|c\|_{L^2(\Omega)}$ and $\|c - c_h\|_{L^\infty(\Omega)}/\|c\|_{L^\infty(\Omega)}$ are computed, where c denotes the exact solution. We also compute the *conservation error* $\int_\Omega (c - c_h)\mathrm{d}x$ and the two following error measures (see [3,47]):

$$\text{Dissipation error} = [\sigma(c) - \sigma(c_h)]^2 + (\bar{c} - \bar{c}_h)^2,$$

$$\text{Dispersion error} = 2\left[\sigma(c)\sigma(c_h) - \frac{1}{|\Omega|}\int_\Omega (c - \bar{c})(c_h - \bar{c}_h)\mathrm{d}x\right],$$

where, for a function ϕ, we set

$$\bar{\phi} = \frac{1}{|\Omega|}\int_\Omega \phi\,\mathrm{d}x, \quad \sigma(\phi) = \sqrt{\frac{1}{|\Omega|}\int_\Omega (\phi - \bar{\phi})^2\,\mathrm{d}x}.$$

5.1. One-dimensional advection

In this section, we consider problem (15) with $u = 1$ on the space–time domain $[-1, 1]\times[0, 2]$. In applying SLDG method to this problem, backward trajectories and flux integrals are evaluated exactly. For ease of comparison with the results reported in [23], the L^∞ and L^1 absolute error norms are computed in this case, as well as the maximum and minimum values of the approximate solution. For the first test we set $c_0(x) = \sin(\pi x)$ and consider $\mathbb{P}_1$ and $\mathbb{P}_2$ elements on several computational grids with an increasing number of elements N_{el} and a constant Courant number $C = 0.8$. Table 1 shows the computed error norms for both the NM and M versions of SLDG with $\mathbb{P}_1$ elements. It can be checked that, in absence of monotonization, the proposed scheme is second order accurate in both L^∞ and L^1 norms, while introducing the monotonization the full second order accuracy can only be retained in the L^1 norm. As for the absolute values of the error, we observe that, with respect to the results reported in [23], the limited SLDG method lies in between the reference TVD scheme and the *essentially nonoscillatory* "UNO2" scheme. The monotonic computed solution and the exact solution in the case $N_{\mathrm{el}} = 20$ are shown in Fig. 2, where it can be seen that local extrema are mostly responsible for the loss of second order accuracy. Table 2 shows the computed error norms for both the NM and M versions of SLDG with $\mathbb{P}_2$ elements. In absence of monotonization, the novel scheme appears to be third order accurate, while the introduction of the FCT monotonization reduces the convergence rate. This reduction of the convergence rate is due to errors localized at local extrema, as can be checked from the third and sixth columns of Table 2, where the two intervals $[-0.6, -0.4]$ and $[0.4, 0.6]$ are not considered in the error evaluation.

As second and third test cases, we consider discontinuous initial data, namely a square wave profile and the following irregular profile:

$$c_0(x) = \begin{cases} -x\sin(3\pi x^2/2) & \text{in } [-1, -1/3), \\ |\sin(2\pi x)| & \text{in } [-1/3, 1/3], \\ 2x - 1 - \frac{1}{6}\sin(3\pi x) & \text{in } (1/3, 1]. \end{cases}$$

Monotonic solutions computed on grids with 20 and 40 elements and with $C = 0.8$ are shown in Fig. 3, while the corresponding errors are summarized in Table 3. It can be seen that the piecewise constant component $c_{h,0}$ of the monotonic solution is bounded by the extreme values of the initial datum (while the complete solution is not). The results compare well with those reported in [23] for the "UNO2" scheme.

Table 1
Computed L^∞ and L^1 error norms and estimated convergence rate p for both the NM and M versions of SLDG, with $\mathbb{P}_1$ elements and regular initial datum

N_{el}	L^∞ error		L^1 error	
	NM	M	NM	M
10	5.28e−02	1.10e−01	4.74e−02	6.23e−02
20	1.31e−02	4.13e−02	1.16e−02	1.73e−02
40	3.25e−03	1.34e−02	2.84e−03	4.12e−03
80	8.06e−04	3.75e−03	7.02e−04	9.63e−04
160	2.01e−04	1.10e−03	1.75e−04	2.25e−04
320	5.01e−05	3.10e−04	4.35e−05	5.36e−05
p	2.01	1.69	2.02	2.04

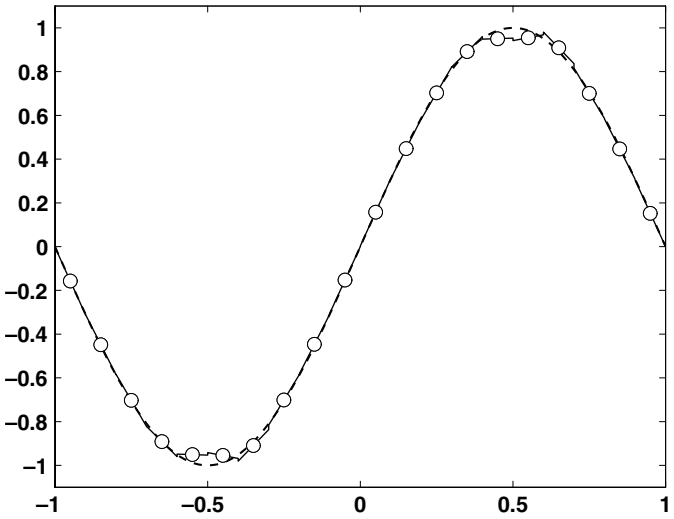

Fig. 2. One-dimensional advection test case with sinusoidal profile, $C = 0.8$ and $N_{el} = 20$. Solid line: piecewise linear SLDG solution; circles: monotonic mean values; dashed line: analytic solution.

Table 2
Computed L^∞ and L^1 error norms and estimated convergence rate p for both the NM and M versions of SLDG, with $\mathbb{P}_2$ elements and regular initial datum

N_{el}	L^∞ error			L^1 error		
	NM	M	M*	NM	M	M*
10	3.35e−03	9.06e−02	5.98e−02	9.95e−04	5.80e−02	3.16e−02
20	4.07e−04	4.17e−02	2.76e−02	1.13e−04	1.51e−02	7.17e−03
40	5.13e−05	1.16e−02	4.08e−03	1.39e−05	2.93e−03	2.39e−04
80	6.43e−06	3.28e−03	1.09e−04	1.73e−06	4.96e−04	4.71e−06
160	8.05e−07	1.13e−03	1.21e−06	2.17e−07	9.06e−05	2.14e−07
320	1.01e−07	5.68e−04	1.01e−07	2.71e−08	2.34e−05	2.57e−08
p	2.99	0.99	3.58	3.00	1.95	3.06

Columns indicated by M^* refer to the monotonic SLDG scheme where the error is evaluated away from local extrema.

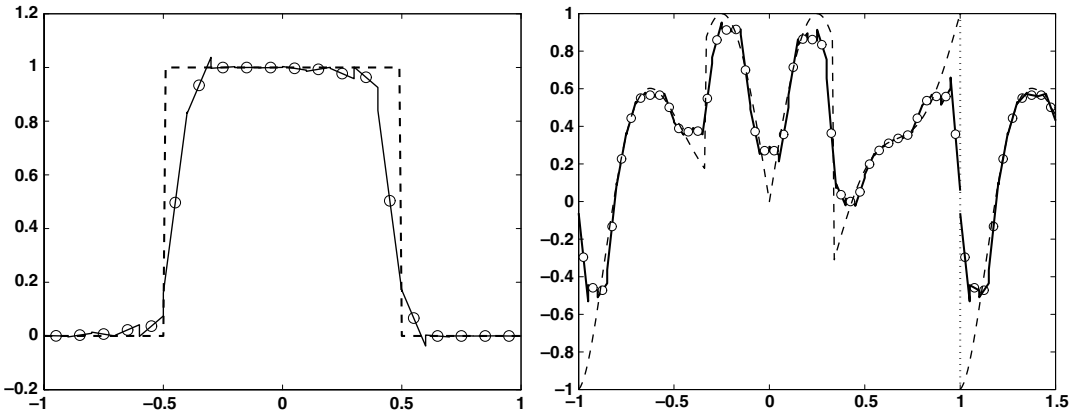

Fig. 3. Left: square wave one-dimensional advection test case with $C = 0.8$ and $N_{el} = 20$: monotonic SLDG solution (solid line, mean values represented by circles), and analytic solution (dashed line). Right: irregular profile one-dimensional advection test case with $C = 0.8$ and $N_{el} = 40$: monotonic SLDG solution (solid line, mean values represented by circles), and analytic solution (dashed line).

Table 3
Error norms for the one-dimensional tests with discontinuous initial data

	Square wave	Irregular profile
L^∞ error	6.98e−01	9.42e−01
L^1 error	1.29e−01	2.16e−01
$\max(c_h)$	1 + 3.77e−02	1 − 4.74e−02
$\min(c_h)$	−3.77e−02	−1 + 4.69e−01
$\max(c_{h,0})$	1 − 4.20e−05	1 − 8.42e−02
$\min(c_{h,0})$	4.20e−05	−1 + 5.28e−01

5.2. Two-dimensional advection: solid body rotation

For the solid body rotation test, a stationary velocity field is considered, representing a rotating flow with frequency $\omega = 2\pi/1000\ \mathrm{s}^{-1} = 6.2832 \times 10^{-3}\ \mathrm{s}^{-1}$ around the point (1, 1) on the spatial domain $\Omega = (0, 2)^2$. The initial datum is either a compactly supported C^3 function with the shape of a cosine hill or a piecewise constant, discontinuous function with the same support, while errors are evaluated at $T = 4000$ s, corresponding to 4 full rotations.

In order to test the accuracy of the proposed SLDG method, we consider the standard test case of solid body rotation with smooth initial datum. Four unstructured computational grids of varying amplitude h are used, keeping the Courant number constant and equal to $C = 0.25$. Numerical quadratures are performed by setting $L_e = 2$, $L_f = 3$ and $M = 2$ in (13). The characteristics of the computational grids are summarized in Table 4 while the numerical results are shown in Table 5 for the nonmonotonic SLDG scheme.

The experimental average convergence rates derived from Table 5 are 2.00, 2.03 in the L^2, L^∞ norms, respectively. Analogous results have been obtained in the L^1 norm. These results appear to be compatible with the supraconvergence estimates presented in [36].

It is interesting to compare the results summarized in Table 5 with the analogous ones obtained using the SL and RKDG formulations under the same working conditions ($C = 0.25$). Table 6 refers to the solution computed by the SL method on three computational grids with $\mathbb{P}_2$ reconstruction, $h = \{0.1, 0.05, 0.025\}$ and number of degrees of freedom $N_{\mathrm{dofs}} = \{2825, 11{,}077, 44{,}665\}$. Table 7 refers to the solution computed by the RKDG method without slope limiting on two computational grids with $\mathbb{P}_1$ finite elements, $h = \{0.1, 0.05\}$ and $N_{\mathrm{dofs}} = \{4116, 16374\}$.

Table 4
Computational grids for the convergence test

h	N_{el}	dofs	Δt
$h = 0.1$	1372	4116	1.25
$h = 0.05$	5458	16374	0.625
$h = 0.033$	12222	36666	0.416
$h = 0.025$	22172	66516	0.312

Table 5
Convergence test for the NM version of SLDG, smooth profile, $C = 0.25$

	Rel. L^2 error	Rel. L^∞ error	Dissipation error	Dispersion error	Conservation error
$h = 0.1$	3.53e−01	4.07e−01	1.96e−02	7.77e−02	−2.54e−16
$h = 0.05$	1.24e−01	1.49e−01	1.51e−03	1.11e−02	−3.92e−16
$h = 0.033$	5.58e−02	6.82e−02	1.96e−04	2.39e−03	1.81e−15
$h = 0.025$	2.73e−02	3.18e−02	3.36e−05	5.87e−04	2.63e−15
	$\min(c_h)$	$\max(c_h)$		$\min(c_{h,0})$	$\max(c_{h,0})$
$h = 0.1$	−4.51e−01	10 − 3.61e+00		−4.26e−01	10 − 4.08e+00
$h = 0.05$	−2.73e−01	10 − 1.05e+00		−2.50e−01	10 − 1.42e+00
$h = 0.033$	−1.21e−01	10 − 4.18e−01		−1.11e−01	10 − 5.72e−01
$h = 0.025$	−5.37e−02	10 − 1.34e−01		−5.04e−02	10 − 2.55e−01

Table 6
Convergence test for SL, smooth profile, $C = 0.25$

	Rel. L^2 error	Rel. L^∞ error	Dissipation error	Dispersion error	Min
$h = 0.1$	7.42e−01	7.13e−01	1.02e−01	1.74e+00	−7.00e−01
$h = 0.05$	5.18e−01	4.86e−01	1.77e−02	8.80e−01	−1.08e+00
$h = 0.025$	2.29e−01	2.14e−01	1.16e−03	1.75e−01	−6.87e−01

Table 7
Convergence test for RKDG without slope limiting, smooth profile, $C = 0.25$

	Rel. L^2 error	Rel. L^∞ error	Dissipation error	Dispersion error	Min
$h = 0.1$	3.47e−01	3.99e−01	2.48e−02	6.91e−02	−2.74e−01
$h = 0.05$	1.15e−01	1.41e−01	2.22e−03	8.55e−03	−1.56e−01

These results show that at low Courant number the SLDG method does not suffer from the error amplification that is typical of SL methods (see e.g. the analysis in [14]), while its accuracy is comparable to that of the RKDG method.

It is now important to evaluate the effects of the limiting procedure on the computed solution. With this aim, we compare the performance of the M version of SLDG method and RKDG method. For the latter, the slope limiting monotonization described in [8] was employed. Results are summarized in Table 8 for the smooth advected profile and in Table 9 for the discontinuous advected profile, respectively. Both cases were computed at resolution $h = 0.1$. It can be noticed that the SLDG method with FCT monotonization is far less diffusive than the slope limiting procedure used in the RKDG formulation. This can be seen also in the plots of the solutions displayed in Fig. 4. It can also be observed that the SLDG solution does not display the excessive sharpening of smooth profiles reported e.g. in [42] in the case of more traditional applications of the FCT technique.

The performance of the SLDG formulation at $C = 3$ is also analyzed. In this case, numerical quadratures are performed by setting $L_e = 8$, $L_f = 6$ and $M = 10$ in (13). Results are summarized in Table 10 for the smooth advected profile without monotonization, computed at resolution $h = 0.05$. The SLDG results are compared to those of a standard SL method with continuous $\mathbb{P}_2$ reconstruction. As is well known, the SL solution is quite sensitive to the trajectory approximation technique. Thus, we report results in two extreme cases of simple Euler approximation with substepping, indicated as SL(a), and of semi-Lagrangian advection computed using the analytical trajectory, indicated as SL(b). In contrast, for the SLDG method only the simple

Table 8
Comparison of SLDG and RKDG with monotonization, smooth profile, $C = 0.25$

	Rel. L^2 error	Rel. L^∞ error	Dissipation error	Dispersion error	Conservation error
SLDG	4.27e−01	5.51e−01	6.25e−02	7.98e−02	−1.04e−15
RKDG	8.05e−01	8.74e−01	3.17e−01	1.89e−01	4.44e−16
	$\min(c_h)$		$\max(c_h)$	$\min(c_{h,0})$	$\max(c_{h,0})$
SLDG	−1.31e−01		10 − 5.39e+00	−2.83e−19	10 − 5.73e+00
RKDG	−1.29e−02		10 − 8.64e+00	2.51e−12	10 − 9.05e+00

Table 9
Comparison of SLDG and RKDG with monotonization, discontinuous profile, $C = 0.25$

	Rel. L^2 error	Rel. L^∞ error	Dissipation error	Dispersion error	Conservation error
SLDG	4.48e−01	6.03e−01	2.18e−01	2.61e−01	−4.74e−16
RKDG	8.04e−01	8.27e−01	9.73e−01	5.75e−01	−1.11e−15
	$\min(c_h)$		$\max(c_h)$	$\min(c_{h,0})$	$\max(c_{h,0})$
SLDG	−1.35e−01		10 − 2.50e+00	−7.33e−19	10 − 3.09e+00
RKDG	−2.13e−02		10 − 7.62e+00	5.75e−12	10 − 8.34e+00

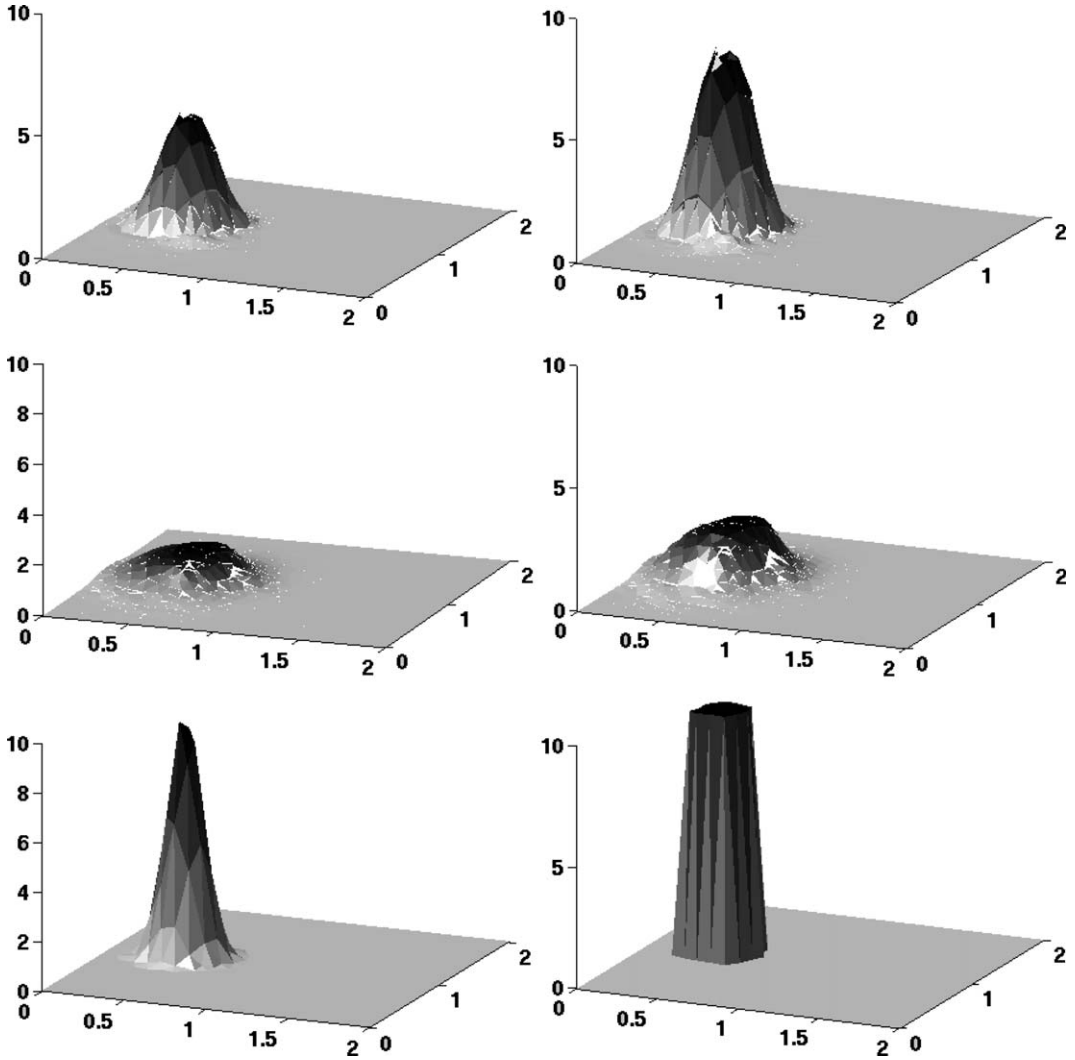

Fig. 4. Monotonized solutions in the solid body rotation test case at $C = 0.25$, smooth profile (left) and discontinuous profile (right). First row: SLDG solution computed with $\mathbb{P}_1$ elements; second row: RKDG solution computed with $\mathbb{P}_1$ elements; third row: analytic solution.

Table 10
Comparison of SLDG with $\mathbb{P}_1$ reconstruction and SL with continuous $\mathbb{P}_2$ reconstruction, smooth profile, $C = 3$

	Rel. L^2 error	Rel. L^∞ error	Dissipation error	Dispersion error	Conservation error
SLDG	7.31e−02	7.20e−02	2.55e−04	4.13e−03	−1.31e−15
SL(a)	2.45e−01	2.44e−01	6.61e−03	4.37e−02	6.93e−02
SL(b)	7.75e−02	7.40e−02	5.51e−04	4.47e−03	−4.20e−03
	$\min(c_h)$	$\max(c_h)$		$\min(c_{h,0})$	$\max(c_{h,0})$
SLDG	−7.68e−02	10 − 5.33e−01		−4.85e−02	10 − 6.70e−01
SL(a)	−2.49e−01	10 − 8.80e−01		−2.36e−01	10 − 9.74e−01
SL(b)	−2.37e−01	10 − 7.59e−01		−2.34e−01	10 − 8.12e−01

Euler approximation is used. It can be seen that the SLDG results are much less sensitive to the trajectory approximation method and that the SLDG errors are comparable to those of SL(b), while they are superior to SL(a). This greater accuracy of SLDG, however, corresponds to a higher computational cost, due to the fact that the numerical solution does not only involve reconstruction at the foot of the characteristic lines, but along these as well.

5.3. Two-dimensional advection: deformational flow tests

Two deformational flow tests are considered. The first one is the nondivergent vortical velocity field introduced in [11], and used by many authors to assess the accuracy of advection schemes, see e.g. [37,38]. The second one is the well-known test proposed by Smolarkiewicz [43].

For the Doswell test problem, a circular domain of radius $R = 3$ is considered, with a triangulation $\mathscr{T}_h$ consisting of 2352 elements with $N_{\text{dofs}} = 7056$. In this case, numerical quadratures are performed by setting $L_e = 12$, $L_f = 6$ and $M = 18$ in (13). The initial datum is a function taking two different constant values on the upper and lower half of the computational domain, respectively, with a sharp transition zone in the middle, and the final time level is $T = 20$. The zero order degrees of freedom representing cell averages are displayed in Fig. 5, as computed by the monotonized SLDG and RKDG schemes, at $C = 2$ and at $C = 0.3$, respectively. It can be observed that the monotonization approach proposed for SLDG leads to a much sharper interface and to much greater detail in the vortex roll-up zone, which is consistent with the error statistics shown in Table 11. Together with the results in the previous section, these test cases lead to the conclusion that the FCT monotonized SLDG method is superior to the standard RKDG method. Furthermore, beyond its application in conjunction to SLDG, the proposed FCT based monotonization technique might also be a useful improvement of monotonization techniques in the framework of generic DG approximations.

For the Smolarkiewicz test problem, we use the SLDG scheme in its NM version on a structured triangulation which fits the boundaries of the convective cells of the flow, as done in the cited reference. Moreover, the orientation of the mesh triangles is chosen in such a way to preserve the symmetry of the problem with respect to the axis $x = 50$. The number of elements is $N_{\text{el}} = 3200$, corresponding to $N_{\text{dofs}} = 9600$, and the time step is chosen in order to have $C = 4$ approximately. In this case, numerical quadratures are performed by setting $L_e = 10$, $L_f = 6$ and $M = 24$ in (13).

As pointed out in [46], where an analytic solution for this test has been described, there are two flow regimes for which different evaluation criteria are appropriate. On a time scale of the order of the characteristic period of the flow, accurate numerical methods are assumed to reproduce the analytic solution correctly. On the other

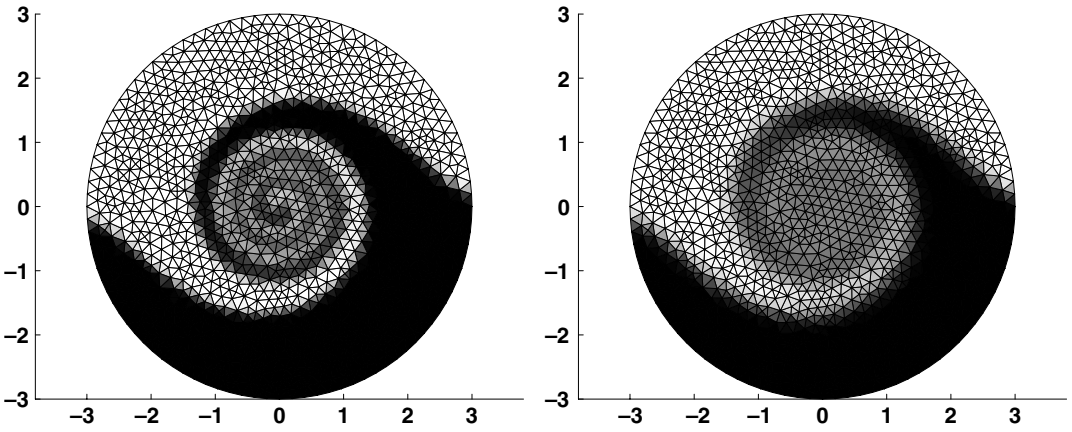

Fig. 5. Doswell deformation flow test case: monotone SLDG solution computed with $\mathbb{P}_1$ elements at $C = 2$ (left) and limited RKDG reference solution computed with $\mathbb{P}_1$ elements at $C = 0.3$ (right).

Table 11
Errors for the SLDG solution ($C = 2$) and RKDG solution ($C = 0.3$) in the Doswell deformation flow test case

	Rel. L^2 error	Rel. L^∞ error	Dissipation error	Dispersion error	Conservation error
SLDG	2.26e−01	1.49e+00	1.02e−03	4.30e−02	−2.75e−15
RKDG	3.61e−01	1.59e+00	1.06e−02	1.01e−01	1.30e−15
	$\min(c_h)$		$\max(c_h)$	$\min(c_{h,0})$	$\max(c_{h,0})$
SLDG	−1 − 4.76e−01		1 + 5.41e−01	−1 − 1.33e−10	1 + 1.00e−13
RKDG	−1 − 7.09e−02		1 + 9.74e−02	−1 − 2.22e−16	1 + 2.22e−16

hand, on a much longer time scale, it can only be expected that the average behaviour of the analytic solution is recovered. Fig. 6(left) illustrates the computed solution at time level $t = 37$ s, corresponding to 3/4 of the characteristic period of the flow, thus in the first regime. Fig. 6(right) shows the computed solution at time level $t = 2500$ s, corresponding to 50 times the characteristic period of the flow, thus in the second regime. The results in the first regime compare well with the plots of the analytic solution presented in [46]. On this time scale, results obtained with the monotonic version of the SLDG method are qualitatively very similar to those shown in Fig. 6. On the longer time scale, the results of the nonmonotonic SLDG scheme are qualitatively similar to large scale average of the analytic solution. The monotonic SLDG scheme yields results (not displayed here) analogous to those of the FCT monotonized scheme discussed in [43].

5.4. Tests on the advection–diffusion equation

In this section, we address the issue of including a discretization of the diffusion term into the SLDG context. Given the structure outlined in the previous sections, the Discontinuous Galerkin methods developed for elliptic problems in [1] appear to be a natural choice. They use the same discontinuous piecewise polynomial representation of the unknown concentration considered for the SLDG method, they guarantee mass conservation at the element level and can reach high order accuracy. In a preliminary implementation, we choose the Interior Penalty (IP) formulation discussed in [1] for the stationary case and applied in [27] to time dependent problems. A simple forward Euler method is considered for the time stepping. This choice results in stability and accuracy restrictions for the overall scheme, whose maximum available time step is dictated by the diffusion process. Other time stepping techniques for the diffusion term could also be considered. Furthermore, it is to be remarked that, for simplicity, diffusive terms are included here by means of an operator splitting approach. We do not consider this an optimal solution and more appropriate ways to deal with the diffusion term in SLDG are currently being investigated. On the other hand, operator splitting is often used to include

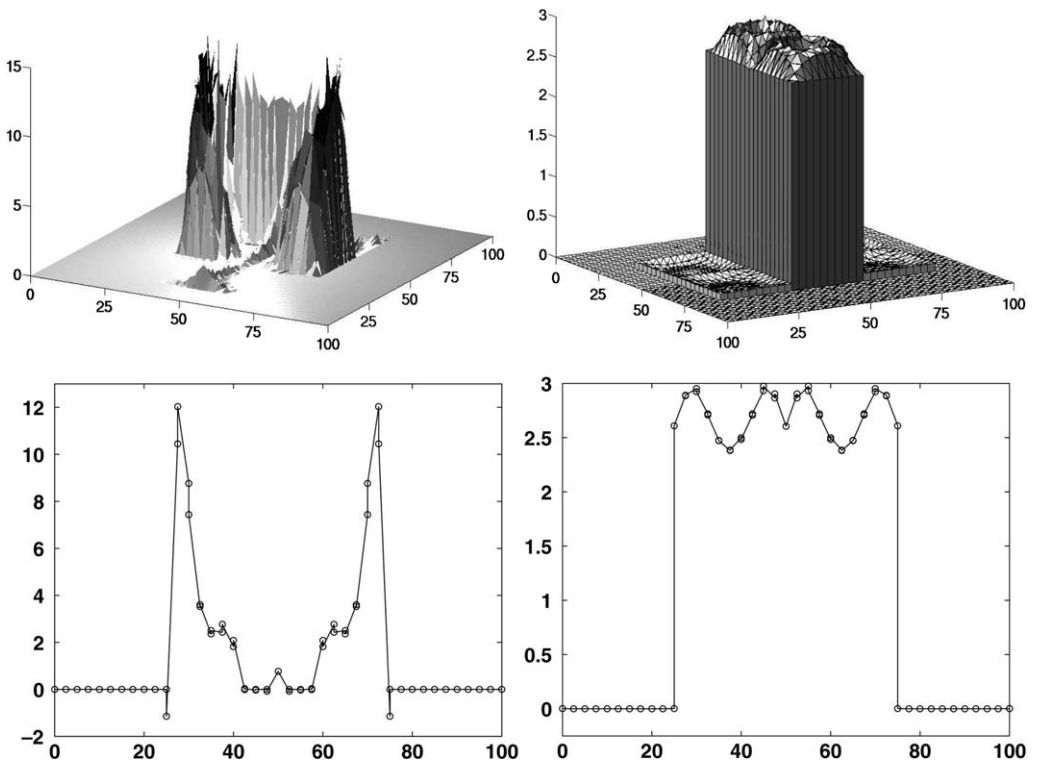

Fig. 6. Smolarkiewicz deformation flow test case. SLDG solution computed with $\mathbb{P}_1$ elements at Courant number 4. Left: time level $t = 37$ s, first flow regime; right: time level $t = 2500$ s, second flow regime. Upper row: three-dimensional plots of the computed solution. Lower row: sections of the computed solution along the middle line of the computational domain.

diffusion in many existing models, so that the present results are an indication of what can be expected if the SLDG formulation is applied within one of these models.

Two numerical experiments are carried out to validate the proposed formulation for advection dominated flow regimes. In both cases, a constant viscosity ν is considered. The first test considers one-dimensional constant velocity advection of an initial Gaussian profile with zero mean and standard deviation $\sigma_0 = 1$ in presence of diffusion. The flow field, the diffusion coefficient and the final time level are chosen in such a way that the final profile has mean and standard deviation equal to $53\sigma_0$ and $3\sigma_0$, respectively. The Péclet number is $UL/2\nu = 343$, where U denotes the magnitude of the advective velocity and L denotes a typical length scale. The Courant number is $C = 1.5$, while $\nu\Delta t/h^2 = 0.16$. The stabilization parameter for the IP scheme is set to 1 and $\mathbb{P}_1$ elements are considered. Results for the M version of SLDG advection are shown in Fig. 7. For the two-dimensional case, the solid body rotation of an initial Gaussian profile is considered with mean (0.5, 1) and standard deviation $\sigma_0 = 0.0427$, under the same setting as in Section 5.2. The grid size is such that the Courant number is approximately equal to $C = 3$. Five rotations are performed and the diffusion coefficient is chosen in such a way that the Péclet number is $UL/2\nu = 3900$ approximately while $\nu\Delta t/A = 0.02$ approximately, where A denotes the average element area. The solution at final time has standard deviation equal to $\sigma_0 = 0.077$. The results for the M version of SLDG advection are shown in Fig. 8. The error norms for both cases are displayed in Table 12. We can observe that the errors obtained are approximately of the same magnitude as in purely advective tests carried out at analogous space–time resolutions (see e.g. Table 10). Mass is conserved up to machine precision and no significant difference is observed when considering the NM version of the scheme. Furthermore, in the two-dimensional test the error in the standard deviation of the computed solution can be estimated at approximately 10% of the exact value. Thus, even considering the limitations of the approach used to introduce diffusion, the resulting method for the advection–diffusion equation appears to be sufficiently accurate for many practical applications.

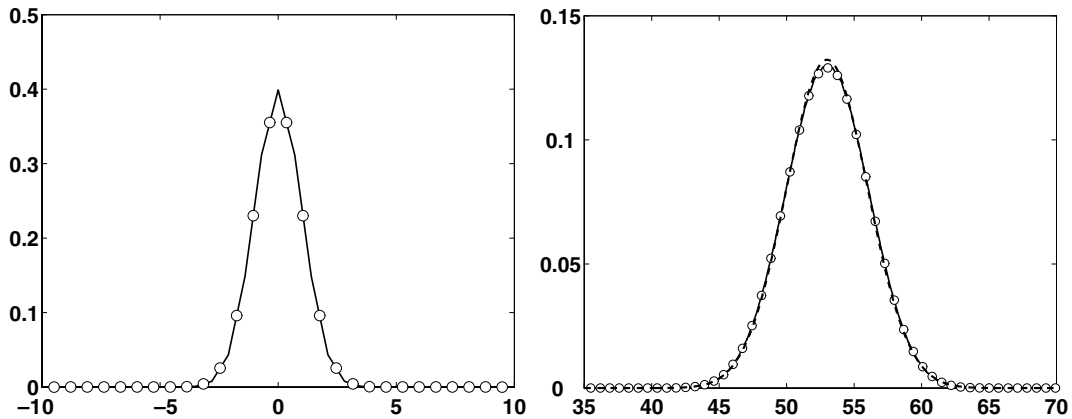

Fig. 7. One-dimensional advection–diffusion test cases. Left: initial datum. Right: computed $\mathbb{P}_1$ solution (solid line, mean values represented by circles) and exact solution (dashed line).

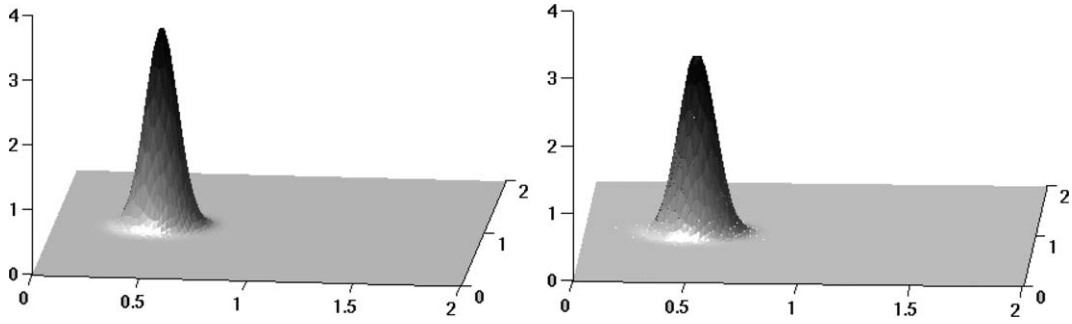

Fig. 8. Two-dimensional advection–diffusion test cases. Left: exact solution. Right: computed $\mathbb{P}_1$ solution.

Table 12
Advection diffusion tests: results obtained with SLDG in one- and two-dimensional cases

	Rel. L^2 error	Rel. L^∞ error	Dissipation error	Dispersion error
1D test	1.68e−02	2.43e−02	2.52e−08	1.44e−07
2D test	7.98e−02	1.44e−01	8.68e−05	1.89e−04

6. Open issues and further developments

One major open issue with respect to the SLDG method appears to be the characterization of the accuracy required in the space–time quadrature formulae introduced in Section 2.4. A precise evaluation of the efficiency of the SLDG method compared to other more mature methods can be feasible only once the above issue is properly addressed. The accuracy required in the quadrature formulae for the approximate computation of the fluxes and volume integrals in equation (5) appears to be related to the local Courant number. Precisely, for low Courant numbers, a smaller number of quadrature points appears to be sufficient to achieve the same level of accuracy, compared to the numbers necessary for higher Courant number cases. One possibility to improve computational efficiency could be to choose the number of quadrature points locally in space and time as a function of the Courant number.

7. Conclusions

In this article, the SLDG discretization approach for the scalar advection equation has been introduced, combining the accuracy and flexibility of the DG method with the computational efficiency and robustness of semi-Lagrangian techniques. Unconditional stability of the proposed discretization has been proved in the von Neumann sense for the one-dimensional case. A monotonization technique has been introduced, based on the Flux Corrected Transport approach, which yields a multi-dimensional monotonic scheme for the piecewise constant component of the computed solution, reducing at the same time the numerical diffusion of monotonization approaches more common in the Discontinuous Galerkin framework. The accuracy and stability of the method have been demonstrated by several one-dimensional and two-dimensional tracer advection tests. In particular, the comparison with results obtained by standard semi-Lagrangian and Discontinuous Galerkin methods has shown that SLDG merges effectively the most desirable properties of both approaches, avoiding at the same time their most remarkable shortcomings. More thorough theoretical analysis and further testing of the proposed approach are currently being undertaken, as well as the extension of the novel scheme to tracer transport in divergent flows and to the solution of nonlinear systems of conservation laws.

Acknowledgements

This research has been supported by the M.U.R.S.T. COFIN Project "Adattività Numerica e di Modello per Problemi alle Derivate Parziali" (2004–2006). We wish to thank J. Behrens, E.S. Gross, T. Ringler, G. Rosatti and W. Sawyer for several discussions on conservative semi-Lagrangian methods over the last few years. The helpful comments of F. Giraldo on a preliminary version of this paper are kindly acknowledged, along with the very constructive remarks of two anonymous reviewers. The numerical method presented here is currently being investigated in the framework of the PhD thesis of one of the authors (MR), under the supervision of the other two (LB, RS).

References

[1] D.N. Arnold, F. Brezzi, B. Cockburn, L.D. Marini, Unified analysis of Discontinuous Galerkin methods for elliptic problems, SIAM Journal of Numerical Analysis 39 (2002) 1749–1779.
[2] J.R. Bates, A. McDonald, Multiply-upstream, semi-Lagrangian advective schemes: analysis and application to a multilevel primitive equation model, Monthly Weather Review 110 (1982) 1832–1842.
[3] R. Bermejo, A. Staniforth, The conversion of semi-Lagrangian advection schemes to quasi-monotone schemes, Monthly Weather Review 120 (1992) 2622–2632.

[4] L. Bonaventura, L. Kornblueh, T. Heinze, P. Ripodas, A semi-implicit method conserving mass and potential vorticity for the shallow water equations on the sphere, International Journal of Numerical Methods in Fluids 47 (2005) 863–869.
[5] L. Bonaventura, T. Ringler, Analysis of discrete shallow water models on geodesic Delaunay grids with C-type staggering, Monthly Weather Review 133 (2005) 2351–2373.
[6] V. Casulli, R.A. Walters, An unstructured grid, three-dimensional model based on the shallow water equations, International Journal of Numerical Methods in Fluids 32 (2000) 331–348.
[7] G. Chavent, B. Cockburn, Consistance et stabilite des schemas LRG pour les lois de conservation scalaires, INRIA Rapport de Recherche 710, INRIA, 1987.
[8] B. Cockburn, S. Hou, C.W. Shu, The Runge–Kutta Local Projection Galerkin Finite Element Method for conservation laws – IV: The multidimensional case, Mathematics of Computation 54 (190) (1990) 545–581.
[9] B. Cockburn, C.W. Shu, The Runge–Kutta local projection P1 Discontinuous Galerkin method for scalar conservation laws, Mathematical Modelling and Numerical Analysis 25 (1991) 337–361.
[10] B. Cockburn, C.W. Shu, The Runge–Kutta Discontinuous Galerkin method for conservation laws, V, Journal of Computational Physics 141 (1998) 198–224.
[11] C.A. Doswell, A kinematic analysis of frontogenesis associated with a nondivergent vortex, Journal of the Atmospheric Sciences 41 (1984) 1241–1248.
[12] J.K. Dukowicz, J.R. Baumgardner, Incremental remapping as a transport/advection algorithm, Journal of Computational Physics 160 (2000) 318–335.
[13] R.E. Ewing, H. Wang, A summary of numerical methods for time-dependent advection-dominated partial differential equations, Journal of Computational and Applied Mathematics 128 (2001) 423–445.
[14] M. Falcone, R. Ferretti, Convergence analysis for a class of semi-Lagrangian advection schemes, SIAM Journal of Numerical Analysis 35 (1998) 909–940.
[15] M. Fey, Ein echt mehrdimensionales Verfahren zur Lösung der Eulergleichungen, Dissertation 10034, ETH, 1993.
[16] M. Fey, Multidimensional upwinding. Part i: The method of transport for solving the Euler equations, Journal of Computational Physics 143 (1998) 159–172.
[17] M. Fey, Multidimensional upwinding. Part ii: Decomposition of the Euler equations into advection equations, Journal of Computational Physics 143 (1998) 181–199.
[18] P. Frolkovic, Flux-based method of characteristics for contaminant transport in flowing groundwater, Computing and Visualization in Science 5 (2002) 73–83.
[19] P. Frolkovic, Flux-based methods of characteristics for coupled transport equations in porous media, Computing and Visualization in Science 6 (2004) 173–184.
[20] F.X. Giraldo, Trajectory computations for spherical geodesic grids in cartesian space, Monthly Weather Review 127 (1999) 1651–1662.
[21] F.X. Giraldo, The Lagrange–Galerkin for the two-dimensional shallow water equations on adaptive grids, International Journal of Numerical Methods in Fluids 33 (2000) 789–832.
[22] F.X. Giraldo, Lagrange–Galerkin methods on spherical geodesic grids: the shallow water equations, Journal of Computational Physics 160 (2000) 336–368.
[23] A. Harten, S. Osher, Uniformly high-order accurate nonoscillatory schemes, I, SIAM Journal of Numerical Analysis 24 (April) (1987) 279–309.
[24] C.W. Hirt, A.A. Amsden, J.L. Cook, An arbitrary Lagrangian–Eulerian computing method for all flow speeds, Journal of Computational Physics 14 (1979) 227–245.
[25] L.W. Horowitz, S. Walters, D.L. Mauzerall, L.K. Emmons, P.J. Rasch, C. Granier, X. Tie, J.F. Lamarque, M.G. Schultz, G.P. Brasseur, A global simulation of tropospheric ozone and related tracers: description and evaluation of MOZART, version 2, Journal of Geophysical Research 108 (2003) 4784–4802.
[26] J.P.R. Laprise, R. Plante, A class of semi-Lagrangian integrated-mass (SLIM) numerical transport algorithms, Monthly Weather Review 123 (1995) 553–565.
[27] A. Lasis, E. Süli, *HP*-version Discontinuous Galerkin finite element methods for semilinear parabolic problems, Preprint NI03068, Isaac Newton Institute for Mathematical Sciences, 2003.
[28] B.P. Leonard, A.P. Lock, M.K. MacVean, Conservative explicit unrestricted-time-step multidimensional constancy-preserving advection schemes, Monthly Weather Review 124 (November) (1996) 2588–2606.
[29] R.J. Leveque, High-resolution conservative algorithms for advection in incompressible flow, SIAM Journal of Scientific Computing 33 (2) (1996) 627–665.
[30] S.J. Lin, Richard B. Rood, Multidimensional flux-form semi-Lagrangian transport schemes, Monthly Weather Review 124 (September) (1996) 2046–2070.
[31] W.H. Lipscomb, T.D. Ringler, An incremental remapping transport scheme on a spherical geodesic grid, Monthly Weather Review 133 (2005) 2335–2350.
[32] B. Machenhauer, M. Olk, The implementation of the semi-implicit scheme in cell-integrated semi-Lagrangian models, Atmosphere-Ocean XXXV (1) (1997) 103–126.
[33] B. Machenhauer, M. Olk, Design of a semi-implicit cell-integrated semi-Lagrangian model, in: MPI Workshop on Conservative Transport Schemes: 2–3 June 1997, pp. 76–85. MPI Report No. 265, July 1998.
[34] E. Miglio, A. Quarteroni, F. Saleri, Finite element approximation of quasi-3d shallow water equations, Computer Methods in Applied Mechanics and Engineering 174 (1999) 355–369.

[35] K.W. Morton, On the analysis of finite volume methods for evolutionary problems, SIAM Journal of Numerical Analysis 35 (1998) 2195–2222.
[36] K.W. Morton, E. Süli, Evolution-Galerkin methods and their supraconvergence, Numerische Mathematik 71 (1995) 331–355.
[37] R.D. Nair, J. Coté, A. Staniforth, Monotonic cascade interpolation for semi-Lagrangian advection, Quarterly Journal of the Royal Meteorological Society 125 (1999) 197–212.
[38] R.D. Nair, B. Machenhauer, The mass-conservative cell-integrated semi-Lagrangian advection scheme on the sphere, Monthly Weather Review 130 (2002) 649–667.
[39] A. Quarteroni, A. Valli, Numerical Approximation of Partial Differential Equations, Springer Verlag, Berlin, 1994.
[40] P.A. Raviart, J.M. Thomas, A mixed finite element method for 2nd order elliptic problems, in: Mathematical Aspects of Finite Element Methods, in: I. Galligani, E. Magenes (Eds.), Lecture Notes in Mathematics, Springer Verlag, Berlin, 1977, pp. 292–315.
[41] G. Rosatti, L. Bonaventura, D. Cesari, Semi-implicit, semi-Lagrangian environmental modelling on cartesian grids with cut cells, Journal of Computational Physics 204 (2005) 353–377.
[42] C. Schär, P.K. Smolarkiewicz, A synchronous and iterative flux-correction formalism for coupled transport, Journal of Computational Physics 128 (1996) 101–120.
[43] P.K. Smolarkiewicz, The multi-dimensional Crowley advection scheme, Monthly Weather Review 110 (1982) 1968–1983.
[44] P.K. Smolarkiewicz, J. Pudykiewicz, A class of semi-Lagrangian approximations for fluids, Journal of the Atmospheric Sciences 49 (1992) 2082–2096.
[45] A. Staniforth, J. Coté, Semi-Lagrangian integration schemes for atmospheric models – A review, Monthly Weather Review 119 (1991) 2206–2223.
[46] A. Staniforth, J. Côté, J. Pudykiewicz, Comments on "Smolarkiewicz's deformational flow", Monthly Weather Review 115 (1986) 894–900.
[47] L.L. Takacs, A two step scheme for the advection equation with minimized dissipation and dispersion errors, Monthly Weather Review 113 (1985) 1050–1065.
[48] C. Timmreck, Three-dimensional simulation of stratospheric background aerosol: first results of a multiannual general circulation model simulation, Journal of Geophysical Research 106 (2001) 28313–28332.
[49] S. Zalesak, Fully multidimensional Flux Corrected Transport algorithms for fluids, Journal of Computational Physics 31 (1979) 335–362.
[50] M. Zerroukat, N. Wood, A. Staniforth, SLICE: a semi-Lagrangian inherently conserving and efficient scheme for transport problems, Quarterly Journal of the Royal Meteorological Society 128 (2002) 2801–2820.